

# Modelling of a Differential Sensor in Eddy Current Non-Destructive Evaluation

Anders Rosell<sup>1,\*</sup> and Gert Persson<sup>2</sup>

<sup>1</sup>Volvo Aero Corporation, <sup>2</sup>Chalmers University of Technology

\*Corresponding author: SE-461 81 Trollhättan, Sweden, anders.ar.rosell@volvo.com

**Abstract:** Interaction between the probe and a defect in eddy current (EC) non-destructive evaluation (NDE) is studied. In this work a differential sensor is considered and the problem regarded here is problem 8 from the testing of electromagnetic analysis methods (TEAM) workshops. The truncation, referring to the position of the outer boundaries of the finite element model, is evaluated in three dimensions (3D) by the use of an analysis in axial symmetry. The results show that it is reliable to use a model size where the positions of the outer boundaries are put where the magnetic vector potential has dropped to 1 % of its maximum value. The axisymmetric model in is compared to an analytical model with good results.

**Keywords:** Eddy current, Non-destructive evaluation, Differential sensor, Calculation of impedance

## 1. Introduction

Modelling is a good tool for understanding and analysing impedance responses due to various flaws, such as cracks and near surface voids or inclusions, in EC NDE. Small impedance variations due to flaw and inspection process must be captured in a model. It is therefore important to use accurate numerical methods. The model size must, however, be minimized in order to carry out efficient computations, especially when related to statistical properties such as probability of detection.

To use methods that comply with these conditions a model with axial symmetry is set up and analysed in a quasi-static magnetic analysis with harmonic fields. This case will first be discussed and compared to an analytical model. The knowledge from this model is then used in the set up and analysis of the more complex case in 3D. Tests are carried out with the position of the outer boundary placed with increasing distance from the EC sensor. Different mesh densities and errors are discussed.

There are several benchmark problems for electromagnetic analysis that have been established in the TEAM workshops [1]. The

goal of these problems is to compare and evaluate simulations of electromagnetic problems. TEAM problem 8 relates to NDE of materials with the EC technique and is used as a framework for the 3D computations within this work. This problem has been experimentally evaluated in [2-4] and evaluated in simulations by different codes in [2-6]. In the work presented here this problem is solved with second order tetrahedral edge elements using COMSOL Multiphysics® with a quasi-static magnetic analysis considering only harmonic fields.

The geometry and set up of TEAM problem 8 is described in figure 1. The parameters and dimension are presented in table 1.

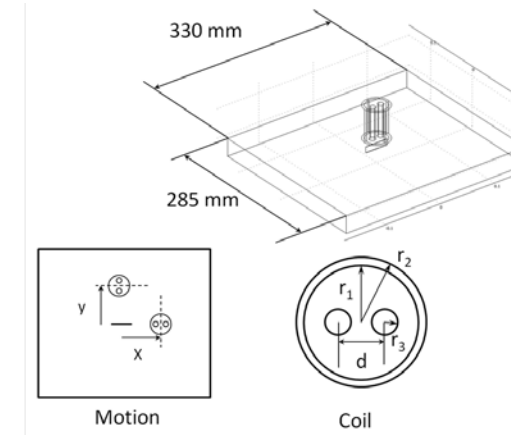


**Figure 1.** Set up of TEAM problem 8 with probe and rectangular defect.

**Table 1.** Parameters and dimensions for the TEAM problem 8.

Sending coil r1	18 mm
Sending coil r2	22 mm
Sending coil length	56 mm
Sending coil lift-off	8 mm
Receiving coil r3	5 mm
Distance d	15 mm
Receiving coil lift-off	9 mm
Receiving coil length	54 mm
Frequency	500 Hz
Defect length	40 mm
Defect depth	10 mm
Defect width	0.5 mm
Block conductivity	1.4 MS/m
Block size	330x 285x 30 mm
Penetration depth	19 mm

The motion of the probe consisting of the outer sending coil and the two differentially connected receiving sensors is indicated in figure 1. The edges of the block must be considered in the model as these influences the signal response of the probe. The computed quantity considered in the problem is the differential impedance signal of the two receiving, sensor coils. The impedance signal is proportional to the difference in magnetic flux within the two coils. Only the shape of the impedance trajectory is considered in this analysis. The probe is moved parallel ( $x$ ) and perpendicular ( $y$ ) to the rectangular defect. The movement of the probe starts from a position over the centre of the defect and ends 80 mm away in both directions. The magnetic flux in a receiving coil is calculated according to

$$\phi = \int_A \mathbf{B} \cdot \hat{n} dS \quad (1)$$

where  $\mathbf{B}$  is the magnetic flux density and  $A$  the area enclosed by the wire in which the electric signal is generated. The differential flux is calculated with and without the flaw corresponding to the states  $\phi_b$  and  $\phi_a$ , respectively for the two receiving coils  $\phi^{(1)}$  and  $\phi^{(2)}$  as

$$\Delta\phi = (\phi_b^{(2)} - \phi_b^{(1)}) - (\phi_a^{(2)} - \phi_a^{(1)}) \quad (2)$$

## 2. Governing equations

Maxwell's equations are the physical model used to solve electromagnetic EC problems. Some approximations are used in this case of problems related to electromagnetic NDE. First the low frequency approximation is used as the wavelengths are long compared to the dimensions of the model. This implies that the displacement currents are neglected as they are small compared to the induced currents. The approximation is implemented by letting  $\epsilon_0$  be equal to zero and thus ignoring the displacement current. This is due to the high electrical conductivity and low frequencies used in problems concerning the EC method in NDE. The Maxwell's equations in term of a quasi-static formulation using the magnetic vector potential gives

$$\nabla \times (\mu^{-1} \nabla \times \mathbf{A}) + j\omega\sigma\mathbf{A} = \mathbf{J}_s \quad (3)$$

where  $\mathbf{J}_s$  is the source current,  $\omega$  is the angular frequency. This equation describes the EC problem.

EC coil problems often have an axial symmetry. The problem can then be simplified to an equation where the magnetic vector potential only has a component in the circumferential direction  $\mathbf{A} = (0, A_\phi(r, z), 0)$ . Equation (3) then becomes

$$-\frac{\partial^2 A_\phi}{\partial r^2} - \frac{1}{r} \frac{\partial A_\phi}{\partial r} - \frac{\partial^2 A_\phi}{\partial z^2} + \frac{A_\phi}{r^2} + j\omega\sigma\mu A_\phi = \mu J_\phi \quad (4)$$

in case of a homogeneous, isotropic and linear material.

## 3. Analysis in axial symmetry

The choice of outer boundaries plays a role in the accuracy of the resulting signal. If the outer boundaries are placed too far from the coil and defect a larger number of degrees of freedom are introduced in the model. The dimensions of the finite element model must thus be limited, truncating the space around the configuration of the defect and the probe.

### 3.1 Analytical solution

The value of the magnetic vector potential surrounding the probe can in the case of a coil be calculated by an analytical model [7]. A detailed description of this analysis is found in the reference. This analysis was implemented in MATLAB<sup>®</sup> for a coil over a two layer conductor in order to compare results with the numerical solution.

### 3.2 Finite element solution in axial symmetry

The magnetic vector potential surrounding the probe is now also calculated in a finite element model with axial symmetry. The degrees of freedom of the 3D problem are then decreased by the truncation of the third dimension. This allows the outer boundary to be moved away from the probe reducing its influence on the final solution. The dimensions of the TEAM problem 8, considering only the current carrying outer coil, are used in the axisymmetric finite element model. The outer boundary is moved far away from the coil and the final mesh is dense as presented in figure 2 in order to get an as accurate result as possible.

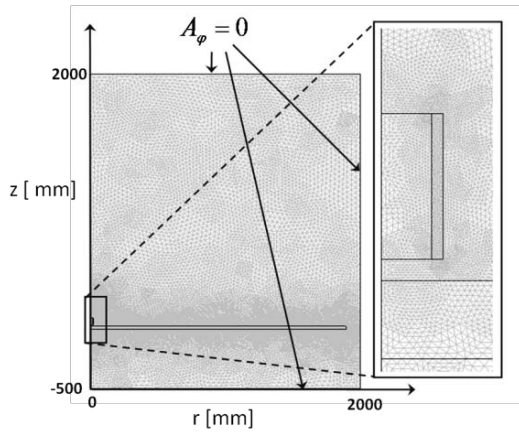


**Figure 2.** Finite element model in axial symmetry.

The solution of the magnetic vector potential is here close to convergence. This is reached in the sense that an increase of the distance between the coil to the outer boundary as well as an increase in the number of elements in the model does not change the solution. The absolute value of the magnetic potential

$$|A_\varphi| = \sqrt{A_\varphi \cdot A_\varphi^*} \quad (5)$$

is used to compare results between the analytical and the numerical solution.

### 3.3 Comparison between analytical and finite element solution

The results are presented in figure 3 as contour curves for the amplitude of the magnetic vector potential. The curves represent 30, 10, 1 and 0.5 % of the maximum amplitude. The result for the finite element model is showed together with the analytical solution.

From the figure it is possible to conclude that there is a good agreement between the analytical model and the axisymmetric finite element solution. It is from this result possible to give input to the 3D analysis when it comes to truncating the model at the outer boundaries.

## 4. Solution to TEAM problem 8

TEAM problem 8 represents a 3D configuration. The edges of the bulk material are influencing the differential signal in the receivers and must be included in the full analysis.

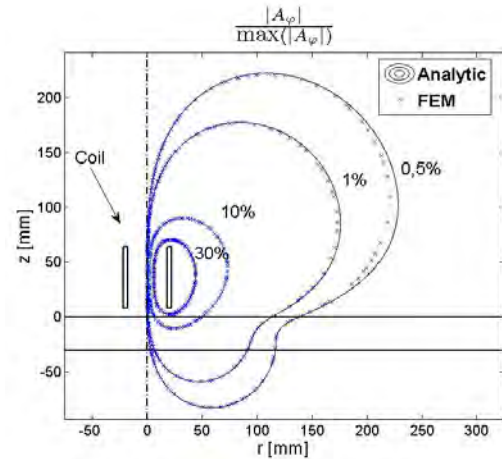


**Figure 3.** Comparison of numerical and analytical solution in axial symmetry. The contour curves show the relative amplitude of the magnetic vector potential.

First we consider the problem without influence from the edges, representing the block as an infinite plate with a thickness of 30 mm. This configuration is used in the axisymmetric model and allows interpretations of the results depending mainly from truncation of the 3D problem. The outer boundaries are an approximation of infinity and must be selected carefully. The results from the model in axial symmetry works as a guideline for the positioning of these boundaries. The position is selected from this experience using the distance from the bottom of the coil carrying external current, the sending coil, to the closest point of the outer boundary. It is convenient to use a rectangular box encapsulating the solution domain and this is used throughout this study.

### 4.1 Impedance of a coil in 3D

The impedance of the sending coil carrying the external current is calculated in order to capture also the behaviour of an absolute single probe. The impedance of a coil can be calculated through dissipated and stored energy assuming that the analysis domain is large enough to capture the major part of the field. The approach for calculation of the impedance cannot be carried out as in the 2D or axisymmetric case considering only the magnetic vector potential of the coil [8]. This is due to the fact that the magnetic vector potential is not constant along the circumference of the coil in the 3D situation. The calculation of impedance from energy considerations results in

$$\begin{aligned}\Delta Z &= Z_b - Z_a = \frac{1}{I^2} \int_S (\mathbf{E}_b \times \mathbf{H}_b^* - \mathbf{E}_a \times \mathbf{H}_a^*) \cdot \hat{\mathbf{n}} dS \\ &= \frac{1}{I^2} \int_V \nabla \cdot (\mathbf{E}_b \times \mathbf{H}_b^* - \mathbf{E}_a \times \mathbf{H}_a^*) dV\end{aligned}\quad (6)$$

where  $Z_b$  and  $Z_a$  represent the impedance with and without the flaw respectively [9]. Here,  $V$  is the total volume of the model and an accurate calculation of impedance is in some sense relying on a capture of the total field built up by the external current in the coil. The impedance as well as the differential signal in the receivers is calculated as the difference between the solution without and with the flaw at each position of the probe.

#### 4.2 Model set up

The axisymmetric model and the 3D model are set up and analyzed using the quasi-static magnetic analysis with harmonic fields. The impedance signal is calculated according to equation (6) for the coil carrying external current and by the use of equation (1) and (2) considering the receiving sensor coils. The computation is at all probe positions done twice. First by setting the electric conductivity in the defect to the same value as the bulk material and then to set it to the value of air, which is zero. For both these computations an identical mesh is used. The computation is then showing the signal difference due to the defect. The use of the same mesh is introduced in order to minimize the errors, which are further discussed in section 4.5. The elements constituting the current carrying coil have zero electric conductivity both in 3D and in the axisymmetric model. The external current is applied in the tangential direction of the sending coil according to figure 4, where the distribution of the induced currents and mesh around the defect are included.

#### 4.3 Position of the outer boundaries in 3D

The results from section 3.3 give an indication of how fast the magnetic vector potential decreases outside the probe. The TEAM problem 8 is first implemented with a defect on a block without edges. Four models with increasing distance between the probe and the outer boundaries are then tested both for the parallel and perpendicular motion of the probe.

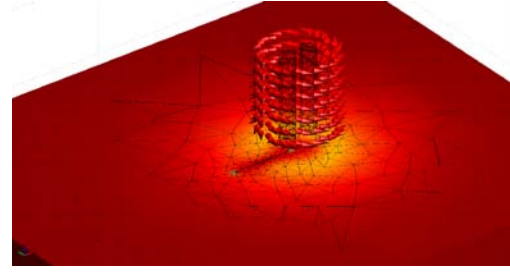


**Figure 4.** Induced current distribution on the surface around the defect.

The reason for excluding the edges of the bulk material first is based on the similarity of the vector potential as compared to the axisymmetric solution. The defect is however present in the 3D case. The four model sizes represent boundary positions where the amplitude of the magnetic vector potential has decreased to 30, 10, 1 and 0.1 %. The result is presented in figure 5 and 6 for parallel and perpendicular motion respectively.

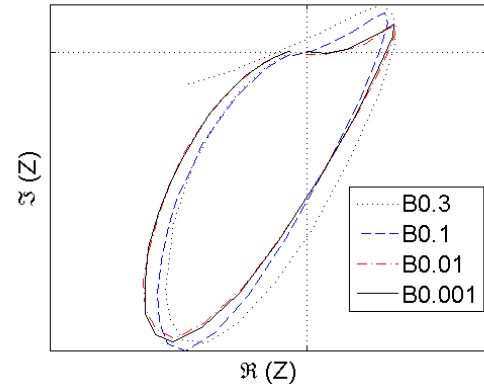


**Figure 5.** Differential signal during motion parallel to the length of the defect. Four positions of the outer boundaries are evaluated. Only the shape of the impedance trajectory is considered.

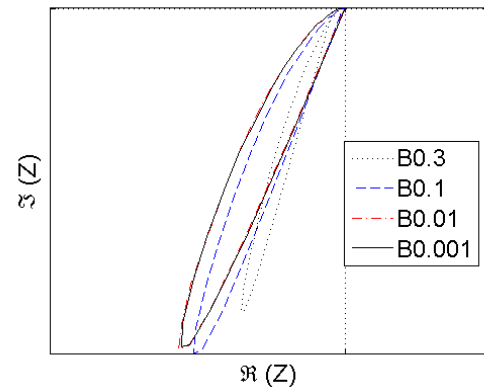


**Figure 6.** Differential signal during motion perpendicular to the length of the defect.

From the figures it is possible to conclude that it is important to put the outer boundaries at sufficient distance from the probe. However, the signal characteristics are captured even with a quite small distance to the boundaries. The signal is close to a converged solution if the outer boundaries are placed at the position where the magnetic vector potential has dropped to about 1 % of its maximum value.

Considering the impedance value of the sending coil calculated from equation (6) it is possible to draw similar conclusions. The result for this analysis is presented in figure 7.

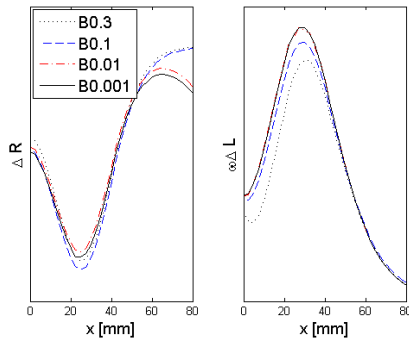


**Figure 7.** Impedance of the sending coil during parallel motion.

#### 4.4 Edge effect

A first approach may be to let the edge of the block be introduced simply as a part of the elements constituting the air. However, in that case the edge effect will be disregarded in computations of the impedance signal using the modelling approach presented here. To avoid this, the edge is considered as a second defect and the signal calculated without the flaw is carried out on a block material that extends out to the boundaries of the model. The resulting differential signal in the receivers is presented in figure 8 and 9 for the scan parallel and perpendicular to the defect respectively.

The figures show that the influence from the edge is present at a distance of approximately 120 mm from the probe axis and has a large impact on the signal. Positions of the probe relative the centre of the defect are included for both the parallel and perpendicular motion in the figures. Resulting impedance of the sending coil with and without the edges in block is presented in figure 10.

The applied mesh is in general selected using principles from appendix A. The mesh M3 presented in table 2 is used throughout this analysis.

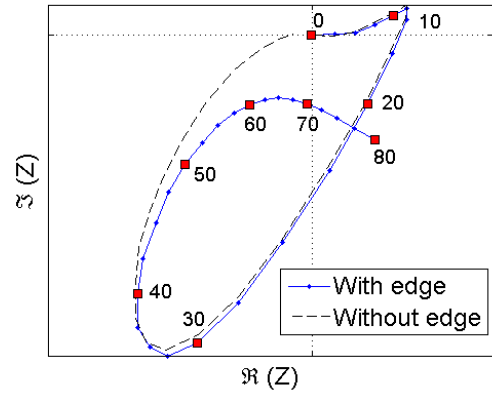


**Figure 8.** Differential signal in the receivers during parallel motion. Probe position relative the center of the defect (mm).

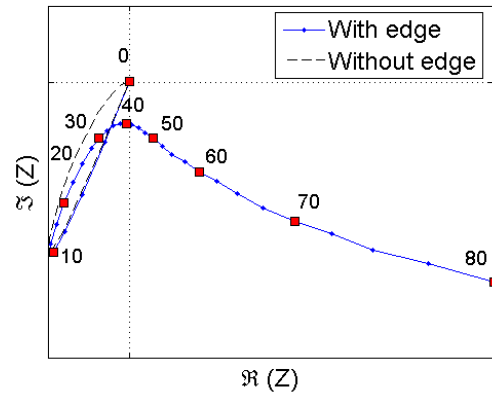


**Figure 9.** Differential signal in the receivers during perpendicular motion. Probe position relative the center of the defect (mm).

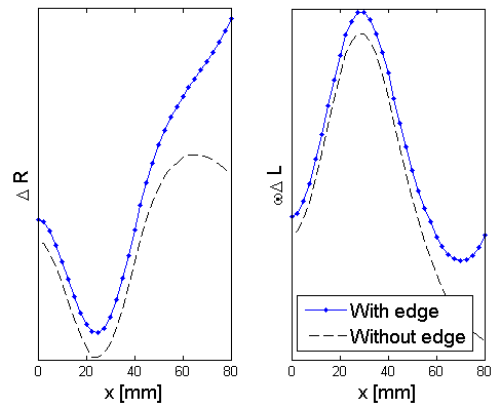


**Figure 10.** Impedance signal in the sending coil during parallel motion.

## 4.5 Errors

The modelled result shows good agreement with previous published experimental and numerical results. It is however important to point out the sources of errors that arise in the modelling scheme presented here. First we assume that the frequency is low, neglecting the displacement current but also describing the applied external current as homogeneous over the cross sectional area of the coil in which the conductivity is zero. This will reduce the influence of resistive losses and capacitive effects in the probe. The computational approach tends however to reduce errors introduced by approximations of the probe as the result relies on the difference of solutions with and without the defect. The second source of error that is important to consider in the finite element analysis is the introduced noise from the non-symmetric mesh. The individual probe positions will not be represented by the same mesh and the differential receivers will have an individual mesh configuration. To further analyze the error the TEAM problem 8 is set up with the sensor rotated 90°. The expected signal is zero impedance difference as the two receivers is placed symmetrically above the defect and block at all positions along the path of the probe. The maximum differential signal under these conditions is however approximately 0.5 % of the maximum amplitude due to the defect. This indicates the numerical error due to the set up of the model. The error grows with a coarse mesh and is about 10 % using M1 presented in figure 11 and table 2 in appendix A.

## 5 Conclusions

The results presented here shows agreement with previous reported numerical and experimental work. The outer boundary should in practice be placed at least at the point where the magnetic vector potential has dropped to 1%. This position can be calculated by a model with axial symmetry. If the computational domain is further decreased, we must expect the modelling error to increase. The mesh density tests show that it is most important to have a fine mesh around the probe. This has an impact on how the external current is described and the region has also the largest impact on signal calculation as this volume has high energy density. A coarse mesh of the probe can give erroneous

prediction when calculating the impedance signal from the flux within the receiving coils. The mesh around the defect has a smaller impact on the computed result. This relates to the fact that all the models studied have an element size of the order of 1-10% compared to the penetration depth in the bulk material.

## References

1. Website: compumag society, compumag.org
2. Bossavit, A. and Verite. The trifou code solving the 3-d eddy current problem by using  $h$  as a state variable, *IEEE Trans. Magn.* **19(6)**, 2465 - 2470 (1983)
3. Takagi, T., Hashimoto, M., Arita, S., Norimatsu, S., Sugiura, T. and Miyata, K. Experimental verification of 3d eddy current analysis code using t-method, *IEEE Trans. Magn.* **26(2)**. 474 - 477 (1990)
4. Verite, J. A coil over a crack. (results for benchmark problem 8 of team workshop), *COMPEL*, **9(3)**, 155–167 (1990)
5. Badics, Z., Matsumoto, Y., Aoki, K., Nakayasu, F., Uesaka, M. and Miya, K. Accurate probe-response calculation in eddy current nde by finite element method, *Journal of Nondestructive Evaluation*, **14(4)**, 181-192 (1995)
6. Song, H. and Ida, N. An eddy current constraint formulation for 3d electromagnetic field calculations, *IEEE Trans. Magn.* **27(5)**, 4012 - 4015 (1991)
7. Dodd, C. and Deeds, W. Analytical solutions to eddy-current probe-coil problems, *Journal of Applied Physics*, **39(6)**, 2829 - 2838 (1968)
8. Ida, N. Alternative approaches to the numerical calculation of impedance, *NDT International*, 21 27–35 (1988)
9. Auld, B.A. and J.C. Moulder. Review of Advances in Quatitative Eddy Current Nondestructive Evaluation. *Journal of Nondestructive Evaluation* **18(1)**, 3–36 (1999)
10. Website, Picasso project (picasso - improved reliability inspection of aeronautic structure through simulation supported pod), <http://www.picasso-ndt.eu>, (2011).

## Acknowledgements

The authors wish to thank Prof. Anders Boström for valuable discussions and for pointing out improvements to this paper. This work is carried out within the European collaboration project Picasso [10]. The support from Volvo Aero and the funding from the

European commission within the FP7 programme are greatly acknowledged.

### Appendix A: Mesh considerations

The finite element mesh influences the computational time, memory usage and computed result. The aim of this study is to conclude how dense the mesh must be and to understand in which region the computational effort should be concentrated. However, if the mesh density is increased in the defect volume this will in turn have an effect on the mesh also in the probe. The aim is to vary the mesh mainly in one of the regions at a time.

The model truncation is put beyond the point where the magnetic vector potential has decreased to 1 % of its maximum amplitude. First we consider the mesh density of the probe. The differential signal in the two receivers is calculated according to equation (2). The number of elements (NOE) in each region is presented in table 2 and the differential flux trajectory in figure 11.

**Table 2.** Number of elements (NOE).

Mesh label	M1	M2	M3	M4
NOE coil	350	530	1264	3902
NOE defect	385	385	385	385
NOE receiver	30	104	296	945
NOE total	6037	7181	12121	25827

Selecting an element density appropriate to model the probe can be concluded from the result in figure 11. The effect of the mesh density of the defect can now be studied. The result from changing the number of elements in the defect region is presented in figure 12 with data presented in table 3.

**Table 3.** Number of elements (NOE).

Mesh label	M5	M6	M7	M8
NOE coil	1264	1264	1264	1265
NOE defect	385	435	1103	4355
NOE receiver	296	296	296	296
NOE total	12165	12426	15032	26831

From figure 11 and 12 it is possible to conclude that it is most important to keep the mesh density high enough to properly resolve the probe. In this case the defect is small or similar in size to the penetration depth which contributes to the insensibility to variations in the number of elements constituting the defect. A small number of elements within the probe

may however give erroneous results. The mesh M3 was used for the analysis in section 4.4.

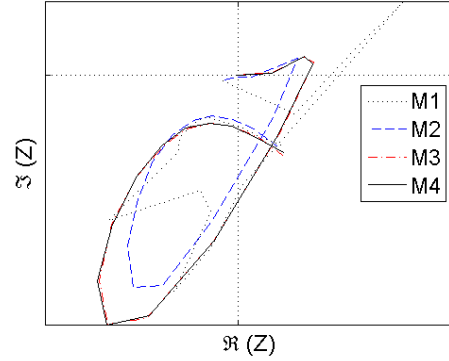


**Figure 11.** Trajectory of the differential signal in the receivers moving parallel to the defect.

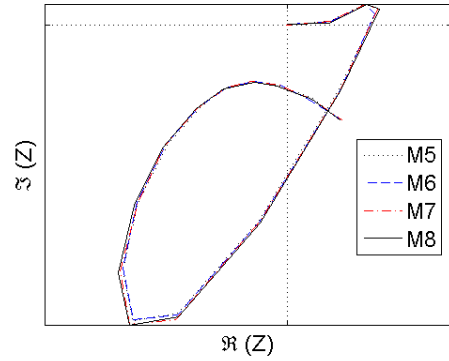


**Figure 12** Trajectory of the differential signal in the receivers moving parallel to the defect.